



CrossMark  
 click for updates

Cite this: *RSC Adv.*, 2016, 6, 23550

## A library of AuNPs modified by RAFT polymers of different charge and chain length: high throughput synthesis and synchrotron XFM imaging using a zebrafish larvae model†

Bao Luan,<sup>abc</sup> Timo Friedrich,<sup>d</sup> Jiali Zhai,<sup>c</sup> Victor A. Streltsov,<sup>c</sup> Benjamin W. Lindsey,<sup>d</sup> Jan Kaslin,<sup>d</sup> Martin D. de Jonge,<sup>e</sup> Jin Zhu,<sup>\*a</sup> Timothy C. Hughes<sup>\*c</sup> and Xiaojuan Hao<sup>\*c</sup>

Gold nanoparticles (AuNPs) have been widely investigated in drug delivery and imaging. However, for such biomedical applications, the modification of AuNPs is necessary to improve their aqueous dispersion stability and biocompatibility, especially in a salt environment. Here, we report a simple and highly efficient method to create a library of polymer-modified gold nanoparticles (PAuNPs) and screen their dispersion stability utilizing high-throughput facilities (in total 1000 experiments). Three types of water soluble polymers with different charge and chain length were prepared using Reversible Addition-Fragmentation chain Transfer (RAFT) polymerization technology. The polymers were then converted into thiol-capped polymers by aminolysis and coated on AuNPs *via* thiol–gold binding to improve aqueous dispersion stability as well as the biocompatibility of AuNPs. Remarkably, we present the first report of imaging zebrafish embryos injected with a PAuNPs sample (selected from our PAuNPs library) using synchrotron X-ray fluorescence microscopy (XFM) beamline. The selected PAuNPs sample, which has been evaluated to be non-cytotoxic to L929 cells and biocompatible to zebrafish larvae in a wide range of concentrations, was injected into zebrafish larvae *via* the cardinal vein and could be clearly visualized in the whole circulatory system including both peripheral blood vessels and the head region by XFM. The result indicates that zebrafish larvae could be a potential animal model for probing the ability of AuNPs to cross the blood–brain barrier (BBB) and therefore hold promise for investigating AuNPs in biomedical applications such as detecting cancer and Alzheimer's disease (AD).

Received 30th January 2016  
 Accepted 23rd February 2016

DOI: 10.1039/c6ra02801b

[www.rsc.org/advances](http://www.rsc.org/advances)

### Introduction

Neurological diseases are becoming a major health problem worldwide with the increased lifespan of humans.<sup>1,2</sup> Among these disorders, Alzheimer's disease (AD) significantly damages and eventually destroys brain cells, leading to the loss of memory function, which over time becomes a burden on families and society.<sup>3</sup> The World Health Organization has estimated that the total number of people with AD worldwide in 2010 was 35.6 million and it nearly doubles every 20 years.<sup>4</sup> Although many new medicines are under development for the

treatment of AD, their access to the central nervous system (CNS) is regulated by the blood–brain barrier (BBB), constituted by a monolayer of endothelial cells that insulates the CNS from the other parts of the body, thus providing a stable environment for neuronal function.<sup>5–7</sup> The effective treatment of AD demands effective drug delivery to the brain. Such transport is heavily limited by the BBB, which prevents greater than 98% of small molecules and 100% of large molecule pharmaceuticals to be potential treatment drugs.<sup>3</sup>

Translating advances in nanotechnology to the medical field has in recent years shown a great potential to play an important role in the diagnosis and treatment of diseases.<sup>8–12</sup> Gold nanoparticles (AuNPs) have recently attracted much interest for their use as carriers for drug delivery because of several unique chemical and physical features, such as functional versatility, biocompatibility, low toxicity, and potentials as contrast agents for computed tomography and photo acoustic medical imaging.<sup>13–23</sup> Several AuNPs systems have been reported to accumulate in the CNS, indicating their ability to cross the BBB and thus potential to treat patients with AD.<sup>24–31</sup> A number of strategies are proposed to achieve the transcytosis of

<sup>a</sup>Chengdu Institute of Organic Chemistry, Chinese Academy of Sciences, Chengdu 610041, China

<sup>b</sup>Graduate University of Chinese Academy of Sciences, Beijing 100049, China

<sup>c</sup>CSIRO Manufacturing, Clayton, Victoria, 3168, Australia. E-mail: Xiaojuan.hao@csiro.au

<sup>d</sup>Australian Regenerative Medicine Institute, Monash University, Clayton, Victoria, 3168, Australia

<sup>e</sup>Australian Synchrotron, Clayton, Victoria, 3168, Australia

† Electronic supplementary information (ESI) available. See DOI: 10.1039/c6ra02801b

therapeutic agents across the BBB.<sup>32</sup> A common method is to couple targeting agents to nanoparticles in order to seek receptor-mediated transcytosis.<sup>30</sup> It is known that the size and chemical nature of the nanoparticle surface affect transcytosis over the BBB<sup>24–26,33,34</sup> Y. S. Chen *et al.* reported that AuNPs of 17 nm passed through the BBB more rapidly than 37 nm, indicating the size-dependency for the ability crossing the BBB.<sup>35</sup> In addition, compared to anionic AuNPs, cationic AuNPs have a higher affinity for the negatively-charged cell surface residues.<sup>33</sup> A recent study reported the effect of AuNPs size and the modifier polyethylene glycol (PEG) molecular weight on the ability to cross the BBB, which demonstrated that a short PEG chain length (MW 1000–2000) in combination with the smallest gold core size led to optimal permeation in their model system.<sup>28</sup> Broadly speaking, the ability of AuNPs to cross the BBB could be affected by the size of gold cores and the property of coating polymers, such as charge and molecular weight.

Various polymers used to modify AuNPs have play an important role in advanced material applications.<sup>36–47</sup> The polymers grafted on the surfaces of AuNPs *via* gold–sulfur bonds or physical interaction can both enhance the stability of gold cores and functionalize the gold cores depending on the unique properties of outside polymer layers.<sup>48–52</sup> For example, the thiolated poly(*N*-isopropylacrylamide) modified AuNPs showed remarkable temperature sensitivity and polymers containing weak acidic or basic groups, such as poly(4-vinylpyridine) modified AuNPs exhibited pH-sensitivity.<sup>49,53</sup> PEG modified AuNPs showed good water solubility, biocompatibility, antibiofouling and other functions.<sup>54–56</sup> Reversible Addition-Fragmentation chain Transfer (RAFT) polymerization has been studied intensively in the past decades, because it allows the preparation of complex polymer architectures including block, graft, comb, and star structures with pre-determined molecular weight, terminal functionality, and narrow molecular weight distribution.<sup>57,58</sup> The RAFT polymer modified nanoparticles have exhibited a great potential in such applications as drug delivery vectors, and imaging contrast agents.<sup>59,60</sup>

In bio-fields, animal models are used to evaluate the performance of biomaterials (including bionanomaterials) in the treatment of human diseases which is important for developing and testing new therapeutics. Animal models, such as the mouse, have been pre-eminent in modeling human diseases. However, several aspects of murine biology limit its use in large scale genetic and therapeutic screening.<sup>61</sup> Alternatively, zebrafish (*Danio rerio*) is becoming a popular vertebrate model for studying human diseases and for evaluating the effects of small molecules on complex physiological and pathological processes.<sup>61–65</sup> External fertilization of zebrafish embryos readily allows access to all developmental stages and provides the feasibility of large scale, high throughput screening strategies, which cannot be achieved in other vertebrate systems. There is growing literature providing evidence that many biomaterials show similar pharmacological effects in zebrafish as they do in mammals. In 2007, a study demonstrated that endothelial tight function-based BBB of zebrafish was similar to that of higher vertebrates, which makes zebrafish

an excellent genetic and experimental model organism for studying BBB permeability.<sup>66</sup>

Herein we present the first report of imaging zebrafish embryos injected with polymer coated AuNPs (PAuNPs) using synchrotron X-ray fluorescence microscopy (XFM) beamline. By that taken, we have firstly developed a library of PAuNPs. RAFT polymerization technology was used to prepare polymers with different charge and chain length, followed by the removal of RAFT end group to generate thiol end group. All polymers were individually used to modify AuNPs and the effect of modification in terms of interaction between polymers and AuNPs and the stability of generated PAuNPs in three media were examined using high throughput plate readers. High throughput methods ensure fast screening of nanomaterials. Based on the outcome of high throughput screening, three selected phosphate-buffered saline (PBS) stable PAuNPs formulations were evaluated for their cytotoxicity using mouse L929 cell line, which showed negligible cytotoxicity within a wide concentration range. Further, one from the three formulations was selected for biocompatibility evaluation in zebrafish larvae, which were both fed and injected with the material. The PAuNPs injected zebrafish larvae were successfully imaged at the Australian Synchrotron using the XFM beamline to detect the distribution of PAuNPs in zebrafish larvae, which, to the best of our knowledge, is the first trial in this field. PAuNPs could be visualized in the whole circulatory system including both peripheral tissues and the head region. Taken together, these preliminary findings recommend zebrafish larvae as a potential animal model for probing the ability of AuNPs to cross the BBB.

## Experimental section

### Reagents and materials

The following reagents and materials were purchased from Sigma-Aldrich, including gold chloride trihydrate ( $\text{HAuCl}_4 \cdot 3\text{H}_2\text{O}$ ; 99.9%), sodium borohydride ( $\text{NaBH}_4$ ; 99.99%), [3-(methacryloylamino)propyl]trimethylammonium chloride solution (MAPTAC; 50 wt% in water), 3-sulfopropyl methacrylate potassium (SPMA; 98%), poly(ethylene glycol) methyl ether methacrylate (PEGMA,  $M_n$  300), inhibitor removers, 4,4'-azobis(4-cyanovaleric acid) (V501; 75%), 4-cyano-4-(phenylcarbonothioylthio) pentanoic acid (chain transfer agent CTA1; 97%), 4-cyano-4-(dodecylsulfanylthiocarbonylsulfanyl) pentanoic acid (CTA2; 97%), PBS (pH 7.4), hexylamine (99%), hydrazine monohydrate, and ethyl 3-aminobenzoate methanesulfonate (tricaine). MAPTAC was purified by removing inhibitor and water and PEGMA was passed through a plug of inhibitor removers prior use. V501 was recrystallised from ethanol twice prior use. PBS was diluted 10 times in Milli-Q water before use. The other materials were used as received. Sodium citrate dihydrate ( $\text{Na}_3\text{C}_6\text{H}_5\text{O}_7 \cdot 2\text{H}_2\text{O}$ ) was purchased from Ajax Finechem. Dialysis tubes (MWCO 1k and 3.5k) were purchased from Spectrum Labs. Gibco Dulbecco's modified Eagle's medium (DMEM), fetal bovine serum (FBS), and glutaMAX™ were purchased from Life Technologies. Acetone, methanol, ethanol were purchased from Merck.

### Synthesis of PMAPTAC, PSPMA, P(PEGMA) *via* RAFT process

As a typical procedure, the synthesis of poly[3-(methacryloylamino) propyl]trimethylammonium chloride (PMAPTAC) with 5k molecular weight (MW) was conducted with the feed molar ratio of [MAPTAC]/[CTA2]/[V501] at 220/5/1. MAPTAC (2.00 g, 9.06 mmol), CTA2 (83.1 mg, 0.206 mmol), V501 (11.5 mg, 0.041 mmol), and ethanol (3 mL) were mixed and transferred into a microwave reactor vial, equipped with a Spinbar and sealed. The reaction mixture was purged with ultra-high purity argon for 30 minutes. The vial was then placed in an oil bath set at 70 °C for 145 minutes with stirring. The polymerization was terminated by placing the vial in an ice bath for 10 minutes. Proton nuclear magnetic resonance (<sup>1</sup>H NMR) spectroscopy was used to determine the conversion of the monomer by comparing the integrity of vinyl proton peaks to that of aliphatic proton peaks. The crude polymer was purified by precipitation in diethyl ether (200 mL) three times followed by filtration and the collected powder was dried in a vacuum oven at room temperature to yield a light yellow powder. Polymer purity was confirmed by <sup>1</sup>H NMR spectroscopy through the absence of monomer peaks. A similar procedure was followed for the synthesis of poly(3-sulfopropyl methacrylate potassium) (PSPMA), and poly[poly(ethylene glycol) methyl ether methacrylate] (P(PEGMA)), but with variations in CTA species, feed molar ratio of monomer/CTA/initiator, reaction time, and solvents for reaction and precipitation. The details of the polymerization conditions are presented in Table 1.

### Synthesis of thiol-capped polymers

RAFT end groups were cleaved off by an aminolysis reaction to produce corresponding thiolated poly[3-(methacryloylamino) propyl] trimethylammonium chloride (**P<sub>a</sub>**), poly(3-sulfopropyl methacrylate potassium) (**P<sub>b</sub>**), and poly[poly(ethylene glycol) methyl ether methacrylate] (**P<sub>c</sub>**), corresponding to PMAPTAC, PSPMA, P(PEGMA) prepared *via* RAFT process. As an example, PMAPTAC prepared by CTA2 was dissolved in ethanol and 30 equivalents of hydrazine hydrate were added under argon atmosphere at room temperature. The mixture was stirred for

10 hours. UV-visible spectroscopy was used to monitor the disappearance of the absorption peak at wavelength of 308 nm which originated from the thiocarbonyl group. Its complete disappearance indicates the removal of the RAFT end group. The resulting crude **P<sub>a</sub>** was purified by dialysis against water for 2 days (change water every 12 hours) followed by freeze-drying to yield white powder. P(PEGMA) or PSPMA prepared by CTA1 was dissolved in ethanol or water separately and 3 equivalents of hexylamine was added under argon atmosphere at room temperature. The mixture was stirred for 2 hours at room temperature until the pink colour disappeared. The resulting crude **P<sub>b</sub>** or **P<sub>c</sub>** was purified by precipitating into ethanol or cyclohexane. By monitoring the disappearance of phenyl group in <sup>1</sup>H NMR spectra and disappearance of absorption peak at wavelength of 308 nm, the complete removal of the RAFT end group was confirmed.

### Preparation of spherical citrate-stabilized gold nanoparticles

Spherical AuNPs with average diameters of 32 nm and 19 nm were prepared as previously described.<sup>67</sup> AuNPs with average diameters of 11 nm and 4 nm were prepared following a modified procedure.<sup>28</sup> In detail, for synthesising 11 nm AuNPs, 0.01 M sodium citrate solution (5.4 mL) was added in 0.541 mM HAuCl<sub>4</sub> solution (200 mL) at room temperature and the mixture was stirred for 5 minutes. 0.1 M fresh NaBH<sub>4</sub> solution (4.3 mL) was rapidly added to the above mixture. The reaction was allowed for 2 hours with stirring, resulting in the final reaction mixture containing 11 nm AuNPs as an orange solution. AuNPs of 4 nm were prepared following the same Au/citrate ratio as that used for making 11 nm AuNPs, but using an altered Au/borohydride ratio. In this case, 200 mL 0.541 mM HAuCl<sub>4</sub> solution, 5.4 mL 0.01 M sodium citrate solution and 10.8 mL 0.1 M fresh NaBH<sub>4</sub> solution were used.

### Modification of AuNPs by **P<sub>a</sub>**, **P<sub>b</sub>** and **P<sub>c</sub>**

Thiolated polymers **P<sub>a</sub>**, **P<sub>b</sub>** and **P<sub>c</sub>** were used to modify AuNPs following a general procedure as described below. AuNPs solution (0.06 mg mL<sup>-1</sup>) and polymer solution in a known concentration were mixed in a glass vial and incubated for 12

Table 1 Summary of RAFT polymerization conditions for PMAPTAC, PSPMA and P(PEGMA)

	Target $M_n$	CTA	$[M]/[CTA]/[I]^a$	Reaction solvent	Reaction time (min)	Proton peaks for monomer conversion determination (ppm)	Precipitation solvent
PMAPTAC	5k	CTA2	220/5/1	Ethanol	145	5.72, 5.47, 3.40, 3.18	Diethyl ether
	10k		445/5/1		120		
	15k		445/5/1		360		
PSPMA	5k	CTA1	195/5/1	Water/ethanol	105	6.01, 5.58, 4.06	Ethanol
	10k		400/5/1		70		
	15k		400/5/1		120		
P(PEGMA)	5k	CTA1	160/5/1	Ethanol	120	6.06, 5.58, 4.07	Cyclohexane
	10k		210/5/1		220		
	15k		495/5/1		120		
	30k		995/5/1		150		

<sup>a</sup> Molar ratio of monomer, CTA and initiator.

hours at room temperature. Three classes of polymers with different charge and molecular weight were used, resulting in 10 polymer samples in total. These polymers were separately mixed with AuNPs of 4 different sizes at a known mass ratio of polymer to AuNPs. To screen the optimal mass ratio of polymer to AuNPs, for each polymer, 5 polymer concentrations were prepared by gradient dilution to make the ratio as 1/9 (C1), 1/3 (C2), 1/1 (C3), 3/1 (C4), and 9/1 (C5), respectively, resulting in the total combinations between AuNPs and polymers to be  $10 \times 4 \times 5 = 200$ . To determine the experimental error, 5 repeating experiments were conducted for each combination. In total, 1000 experiments need to be conducted, which made it an unachievable task within a short time with normal manipulations. Therefore, a high throughput method<sup>68</sup> was used to screen the combinations in order to get the best candidates. In detail, AuNPs solution ( $0.06 \text{ mg mL}^{-1}$ ,  $120 \mu\text{L}$ ) was filled into each well of the 96-well standard microplate (maximum volume of each well is  $200 \mu\text{L}$ ), followed by the addition of  $30 \mu\text{L}$  polymer aqueous solution with a series of concentration ( $0.027$ ,  $0.08$ ,  $0.24$ ,  $0.72$ , and  $2.16 \text{ mg mL}^{-1}$ , respectively). The plate was incubated at a rate of  $100 \text{ rpm}$  at room temperature for 12 hours. The UV-visible absorbance spectra were acquired by FlexStation 3 Multi-Mode Microplate Reader with scanning region from  $260$  to  $720 \text{ nm}$  with a step of  $1 \text{ nm}$ . The hydrodynamic diameters of above polymer/AuNPs mixtures were obtained by Wyatt DLS plate reader. Transmission electron microscopy (TEM) was also used to confirm the modification result obtained from UV-visible and DLS methods.

#### Aqueous dispersion stability test of PAuNPs via high throughput method

Stability test of PAuNPs was conducted by a high throughput approach by monitoring the absorbance change of PAuNPs around surface plasmon resonance (SPR) peak measured on a FlexStation 3 Multi-Mode Microplate Reader. The use of 96-well plates ensured fast measurement and less material per test. The experiments were carried out in three different media: Milli-Q water, PBS, and PBS mixed with  $5 \text{ wt\%}$  bovine serum albumin (BSA). The measurements were acquired at SPR  $528$ ,  $523$ , and  $519$ , as well as  $450 \text{ nm}$ , for the AuNPs of  $32$ ,  $19$ , and  $11 \text{ nm}$  in size, respectively. For instance,  $1 \text{ mL}$  of AuNPs solution ( $32 \text{ nm}$ ) was mixed with  $0.25 \text{ mL}$  of  $\text{P}_c$  solution ( $0.72 \text{ mg mL}^{-1}$ ) and the resulting mixture was incubated with stirring at the speed of  $100 \text{ rpm}$  per minute for 12 hours. The generated PAuNPs were then purified by centrifugation three times with washing between centrifugation processes using Milli-Q water. The supernatant was removed and deposit was re-dispersed in  $60 \mu\text{L}$  Milli-Q water to achieve a concentrated PAuNPs solution. The concentrated PAuNPs solution was divided into three wells of 96-plate equally by a pipette ( $20 \mu\text{L}$  each well) and diluted with  $150 \mu\text{L}$  Milli-Q water, PBS alone, and PBS mixture with  $5 \text{ wt\%}$  BSA. The absorbance data of above solutions was continuously acquired at the wavelengths of  $450$  and  $528 \text{ nm}$  for 48 hours at an interval of every  $30$  minutes at  $37 \text{ }^\circ\text{C}$ .

#### Cell culture and cytotoxicity assessment of PAuNPs

Mouse L929 cell line was used to evaluate cytotoxicity of PAuNPs as follows. The L929 cell line was grown at  $37 \text{ }^\circ\text{C}$  under humidified air containing  $5 \text{ vol\%}$  of  $\text{CO}_2$  in DMEM ( $4.5 \text{ g L}^{-1}$  of glucose) supplemented with  $5 \text{ vol\%}$  of FBS and  $1 \text{ vol\%}$  of glutamax<sup>TM</sup>.<sup>69,70</sup> The L929 cells were seeded in 96-well plates with a density of  $5 \times 10^3$  cells per well in DMEM complete medium for 24 hours. The wells were then treated with PAuNPs solutions in DMEM complete medium with different concentrations of  $100$ ,  $50$ ,  $25$ ,  $12.5$ ,  $6.25$ ,  $3.13 \mu\text{g mL}^{-1}$ . For each concentration, triplet experiments were performed at the same time. After a pre-determined incubation period, the cells were rinsed with PBS buffer solution, and cell viabilities were evaluated *via* the methyl thiazolyl tetrazolium (MTT) assay.  $20 \mu\text{L}$  of MTT stock solution ( $5 \text{ mg mL}^{-1}$  in PBS) was added per well. After 1.5 hours incubation at  $37 \text{ }^\circ\text{C}$ , formazan crystals were dissolved with  $200 \mu\text{L}$  of DMSO after removing the media. The absorbance at  $480 \text{ nm}$  was measured using a Fluostar OPTIMA Microplate reader. The relative cell viabilities were calculated as the ratio of the absorbance of the sample to that of untreated cells ( $100\%$  viability) and were expressed in  $\%$ . The  $10 \text{ v\%}$  DMSO treated cells were used as a positive control. Above assays were repeated three times.

#### Evaluation of PAuNPs application and development in zebrafish larvae

All handling of zebrafish larvae was done in accordance with the ethical guidelines and policies set forth by Monash University and ARMI using standard procedures.<sup>71</sup> Zebrafish embryos were raised and manually dechorionated 2 days post fertilization (DPF). For bath application:  $\text{P}_c$  ( $10\text{k}$ ) modified AuNPs ( $11 \text{ nm}$ ) sample (stock:  $0.05 \text{ mg mL}^{-1}$  in  $\text{H}_2\text{O}$ ) was diluted in standard E3 to obtain a range of concentrations ( $0.005$ – $50 \text{ ng mL}^{-1}$ ).  $30$  embryos were incubated in each concentration in a 6 well plate. For micro-injection: stock solution of above PAuNPs sample was diluted in water to obtain a range of concentrations ( $0.005$ – $50 \mu\text{g mL}^{-1}$ ). A volume of  $1 \text{ nL}$  was injected into the cardinal vein.<sup>72</sup> After application, larvae were incubated for 2 days followed by phenotype assessment [modified from OECD test no. 236: Fish Embryo Acute Toxicity (FET) test].

#### Sample preparation for synchrotron imaging

$\text{P}_c$  ( $10\text{k}$ ) modified AuNPs ( $11 \text{ nm}$ ) samples were applied to 2 DPF embryos as described above. Due to the novelty of the protocol, several iterations of conditions were tested. After two days of incubation, larvae from bath application and injection application were euthanized using solution of  $0.04\%$  tricaine (Westfield, 2000). Half of samples were fixed in  $4\%$  paraformaldehyde diluted in PBS, while the other half kept in PBS ( $2$  hours) to test for potential effects of fixation on particle localization. To test for loss of signal, all conditions were both mounted inside  $0.64 \text{ mm}$  ID silicon nitride capillaries (EW-95820-05, Cole and Parmer, Chatswood, NSW Australia) and with their tails sticking out of  $0.49 \text{ mm}$  ID capillaries (EW-95820-04, Cole and Parmer, Chatswood, NSW Australia). All

capillaries with larvae were then fastened to the stage for imaging, consisting of the following groups containing PAuNPs: bath application-fixed-in capillary (BFC), bath application-fixed-out of capillary (BFO), bath application-fresh-in capillary (BFC), bath application-fresh-out of capillary (BFC), injected-fixed-in capillary (IFC), injected-fixed-out of capillary (IFO), injected-fresh-in capillary (IFrC), injected-fresh-out of capillary (IFrO).

### Imaging of PAuNPs in larval zebrafish using XFM

*In vivo* imaging of PAuNPs within zebrafish larvae was performed using XFM at the Australian Synchrotron in Clayton, Victoria, Australia.<sup>73</sup> The XFM beamline is ideally suited for high-sensitivity imaging of trace metals at a high spatial resolution in biological systems,<sup>74–76</sup> and therefore was appropriate for evaluating the presence or absence of PAuNPs in larval zebrafish following bath application or injection. Previous studies have shown that XFM is a useful approach to investigate subcellular biometals in normal and diseased brains.<sup>77–79</sup> In our study, an incident beam of 15.8 keV was used to induce L-shell ionization of Au, and K-shell ionization of Ni, Mn, Fe, Cr, Cu, Br, and Zn. The beam was focused to a spot of approximately 2  $\mu\text{m}$  full width at half maximum (FWHM) using a Kirkpatrick–Baez mirror pair.<sup>73</sup> Full-spectra data acquisition and imaging of trace metals were executed using the Maia detector system.<sup>80,81</sup> Scan parameters were optimized to maximize visualization and anatomical localization of PAuNPs in larval zebrafish. Typical dwell time was around 2.6 ms per 2  $\mu\text{m}$  pixel.

### Polymer characterization

<sup>1</sup>H NMR spectra of purified polymers were obtained with a Bruker Avance 400 MHz spectrometer (<sup>1</sup>H 400 MHz) in D<sub>2</sub>O and CD<sub>3</sub>OD. For P(PEGMA), gel permeation chromatography (GPC) measurements were performed on a Shimadzu system equipped with a CMB-20A controller system, a SIL-20A HT autosampler, a LC-20AT tandem pump system, a DGU-20A degasser unit, a CTO-20AC column oven, a RDI-10A refractive index detector and with 4 Waters Styragel columns (HT2, HT3, HT4, HT5 each 300  $\times$  7.8 mm) providing an effective molar mass range of (100–4  $\times$  10<sup>6</sup>) and with *N,N*-dimethylacetamide (DMAc) containing 2.1 g L<sup>-1</sup> of lithium bromide (LiBr) as eluent with a flow rate of 1 mL min<sup>-1</sup> at 80 °C. The molar masses in poly(methyl methacrylate) (PMMA) equivalents were obtained from a calibration curve constructed with low dispersity PMMA standards (Polymer Laboratories). A third-order polynomial was used to fit the log  $M_p$  versus time calibration curve, which was approximately linear across the molar mass range from 1020 to 1 944 000 g mol<sup>-1</sup>. For PSPMA, GPC measurements were performed on a Waters Alliance system equipped with an Alliance 2695 Separations Module (integrated quaternary solvent delivery, solvent degasser and autosampler system), a Waters column heater module, a Waters 2414 RDI refractive index detector, a Waters PDA 2996 photodiode array detector (210 to 400 nm at 1.2 nm), and 2  $\times$  Agilent PL-Aquagel columns (PL-Aquagel Mixed H (8  $\mu\text{m}$ )), each 300 mm  $\times$  7.8 mm, providing an effective molar mass range of 6  $\times$  10<sup>3</sup> to 10<sup>7</sup>. Mobile phase buffer was prepared with Milli-Q water with 200 mM sodium

nitrate, 10 mM sodium phosphate and 200 ppm sodium azide. Mobile phase was filtered through 0.45  $\mu\text{m}$  filter. The eluent had a flow rate of 1 mL min<sup>-1</sup> at 30 °C. Number ( $M_n$ ) and weight ( $M_w$ ) average molar masses were evaluated using Waters Empower-3 software. The GPC columns were calibrated with low dispersity polyethylene glycol/oxide (PEG/PEO) standards (Polymer Laboratories) ranging from 233 to 1 016 921 g mol<sup>-1</sup> and molar masses are reported as PEG/PEO equivalents. A 3rd-order polynomial was used to fit the log  $M_p$  vs. time calibration curve, which was near linear across the molar mass ranges.

### Nanoparticles characterization

UV-visible spectroscopy, dynamic light scattering (DLS), and TEM were used to determine the size of original and modified gold nanoparticles as well as the nanoparticle surface modification result.

The UV-visible spectra of AuNPs (0.06 mg mL<sup>-1</sup>) were measured using a Cary 50 Bio UV-visible spectrophotometer (Varian Co., USA) at room temperature.

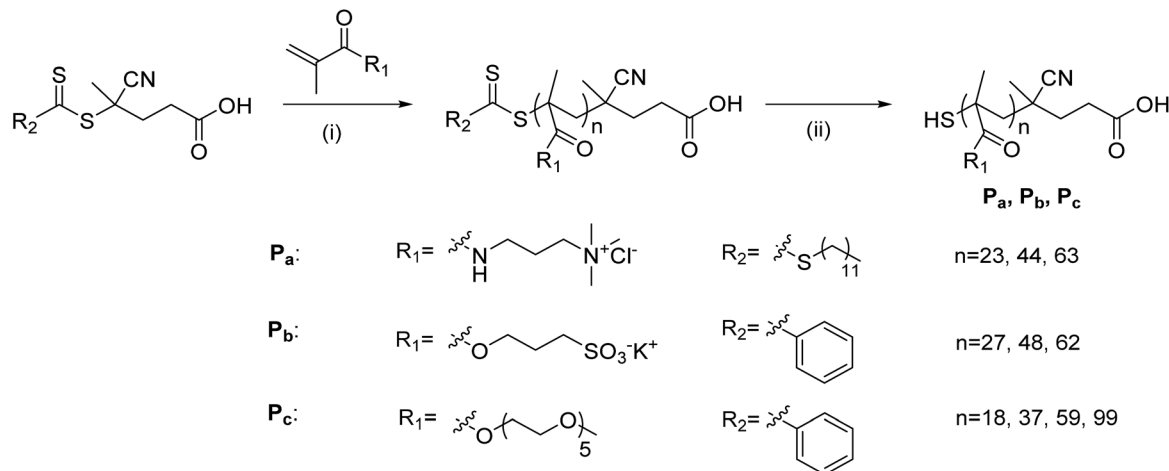
For TEM analysis, carbon-coated 300-mesh copper grids were glow-discharged in nitrogen to obtain hydrophilic carbon film. An aliquot of the sample suspended in water was dropped onto the grid. The sample was either air-dried and examined, or further treated by negative staining prior analysis. Negative staining was conducted as follows: following adsorption of the AuNPs material onto the carbon film for 30 seconds, excess aqueous solution was removed using Whatman 541 filter paper, followed by staining with a drop of aqueous potassium phosphotungstate (2%) at pH 7.2 for 10 seconds. The excess stain was removed by blotting with filter paper as before. Grids were then air-dried before use. The samples were examined on a Tecnai 12 transmission electron microscope (FEI, Eindhoven, Netherlands) at an operating voltage of 120 kV. Images were recorded using a Megaview III CCD camera and AnalySIS camera control software (Olympus).

Dynamic light scattering (DLS) experiments for AuNPs (0.06 mg mL<sup>-1</sup>) were performed using a Malvern Instruments Zetasizer Nanoseries instrument equipped with a 4 mW HeNe laser operating at 633 nm, an avalanche photodiode detector with high quantum efficiency, and an ALV/LSE-5003 multiple  $\tau$  digital correlator electronics system. Measurements were conducted at 25 °C, using automated settings in low-volume cuvettes.

## Results and discussion

### Synthesis of polymers

To investigate how polymer charge affects the modification efficiency and thus influences the aqueous dispersion stability of PAuNPs, three monomers MAPTAC, SPMA, and PEGMA were selected to prepare positively charged, negatively charged, and neutral polymers, respectively. The synthetic route of polymers is shown in Scheme 1. The RAFT technique has been widely used for preparation of a variety of polymers due to its mild conditions and well control over MW and polydispersity.<sup>82,83</sup> Therefore, we have used the RAFT polymerization to prepare



**Scheme 1** Synthesis of RAFT polymers and corresponding thiolated polymers: (i) V501, 70 °C, Ar; (ii) hydrazine hydrate for P<sub>a</sub>, hexylamine for P<sub>b</sub>, and P<sub>c</sub>.

polymers of 5k, 10k, 15k ( $M_n$ ) for each type of monomer with additional 30k for PEGMA (Table 1). To minimize the amount of dead polymer chains formed during the polymerization and thus maximize the latent thiol group content which is needed for gold–thiol bonding in the modification, conversions were controlled between 50 and 75%. The degree of polymerization (DP) of purified polymers was determined by  $^1\text{H}$  NMR spectra based on end group analysis (Fig. S1†). It is worth mentioning that the GPC determined molecular weights (MWs) in this study are relative to PMMA standards and not the true MWs. It is noted that theoretical MWs calculated from conversion are slightly lower than NMR determined MWs, which may indicate that there is a small amount of dead polymer chains present. MWs of PMAPTAC *via* end group analysis by NMR could not be obtained due to the lack of characteristic peaks from the RAFT agent used. Table 2 summarizes information of synthesized polymers.

In addition to the advantage of controlling molecular weight, RAFT polymerization also provides additional functionality *via* the RAFT end group which can be regarded as a protected thiol

group and can be simply liberated by aminolysis reaction. Hexylamine and hydrazine were used to cleave off dithiobenzoate ester and trithiocarbonate end groups, respectively, to generate free thiol groups. After aminolysis process,  $^1\text{H}$  NMR spectra showed absence of phenyl end group for PSPMA and P(PEGMA) (Fig. S1†). In addition, UV-visible spectra showed the disappearance of characteristic absorption peak for thio-carbonyl groups (at 308 nm) after aminolysis (Fig. S2†). GPC traces of the P(PEGMA) before and after aminolysis have shown the absence of any disulfide bond formation (Fig. S3†). In this study, P<sub>a</sub> with different MW will be abbreviated to P<sub>a</sub>5k, P<sub>a</sub>10k, and P<sub>a</sub>15k. Similarly, P<sub>b</sub>5k, P<sub>b</sub>10k, and P<sub>b</sub>15k refer to polymers made from SPMA with  $M_n$  5k, 10k, and 15k, respectively. P<sub>c</sub> with different MW will be referred as P<sub>c</sub>5k, P<sub>c</sub>10k, P<sub>c</sub>15k, and P<sub>c</sub>30k, respectively.

#### Synthesis of AuNPs and characterization

Spherical AuNPs of various sizes (32 nm, 19 nm, 11 nm, and 4 nm) were synthesized *via* the citrate reduction method or modified citrate and borohydride method. UV-visible

**Table 2** Summary of RAFT polymerization results of PMAPTAC, PSPMA and P(PEGMA)

	Target DP	Conversion <sup>a</sup> (%)	$M_n^b$ (based on conversion)	DP <sup>c</sup> (NMR)	$M_n^d$ (NMR)	$M_n^e$ (GPC)	$M_w/M_n^e$ (GPC)
PMAPTAC	44	52.3	5230	N/A	N/A	N/A	N/A
	89	49.0	9800	N/A	N/A	N/A	N/A
	89	70.0	14 000	N/A	N/A	N/A	N/A
PSPMA	39	47.6	4760	27	6920	12 000	1.13
	80	49.2	9840	48	12 090	15 960	1.23
	80	71.4	14 280	62	15 530	19 460	1.09
	32	49.5	4950	18	5680	5650	1.12
P(PEGMA)	42	75.1	9760	37	11 380	8930	1.14
	99	50.5	15 150	59	17 980	12 470	1.12
	199	46.1	27 660	99	29 980	25 050	1.16

<sup>a</sup> Calculated from  $^1\text{H}$  NMR spectrum of polymerization reaction mixture. <sup>b</sup> Calculated from conversion determined by NMR using the equation  $M_n = \text{target DP} \times \text{MW}_{\text{monomer}} \times \text{conversion} + \text{MW}_{\text{RAFT}}$ . <sup>c</sup> DP of PMAPTAC could not be determined by end group analysis, DP of PSPMA and P(PEGMA) was acquired from  $^1\text{H}$  NMR spectra of purified polymer by end group analysis. <sup>d</sup> Calculated from  $^1\text{H}$  NMR DP of purified polymer. <sup>e</sup> PSPMA measured from aqueous GPC, P(PEGMA) measured from DMAc GPC. PMAPTAC: N/A, no polymer signal detected by aqueous GPC.

spectroscopy,<sup>84</sup> DLS<sup>85,86</sup> and TEM were used to characterize the size and homogeneity of AuNPs. As shown in Table 3, the diameter of the particles determined by UV-visible spectroscopy and DLS were in good agreement with TEM negative staining observation (Fig. 1). In addition, the TEM images also showed that most of the gold nanoparticles were spherical. The four batches of AuNPs are labelled as Au<sub>32</sub>, Au<sub>19</sub>, Au<sub>11</sub>, and Au<sub>4</sub> throughout the text, where the subscript shows the gold core diameter determined by TEM.

### Synthesis of PAuNPs and characterization

Polymers with different charge and chain length synthesized *via* RAFT technology were used to modify AuNPs, resulting in numerous combinations. As mentioned above, there were totally 10 polymers and 4 sizes of AuNPs synthesized. Each polymer was coated onto AuNPs at 5 different polymer/Au mass ratios which were 1/9 (C1), 1/3 (C2), 1/1 (C3), 3/1 (C4), and 9/1 (C5), respectively, resulting in 10 (polymers) × 5 (ratios) × 4 (sizes of AuNPs) = 200 (combinations). In addition, to determine experimental error, each combination was repeated 5 times, resulting in 1000 experiments. We used a code system to name so many samples, for example, P<sub>a</sub>5kC1-Au<sub>32</sub> refers to a PAuNPs sample that the AuNPs with size of 32 nm were modified by P<sub>a</sub> of 5k molecular weight at polymer/Au mass ratio of 1/9 (C1). Here, a high throughput method was used to generate a library of PAuNPs containing as many as 200

combinations between polymers and AuNPs. It is not practical to conduct such a huge number of experiments at the bench within a short period of time while the high throughput method indeed provides a shortcut to achieve this by mixing polymer solution and AuNPs solution in a number of 96-well standard micro plates, which not only runs numerous experiments in parallel but also requires a small amount of material. More importantly, the surface modification can be evaluated by automatic measurements of UV-visible spectroscopy using the high throughput UV plate reader. The UV-visible spectra of PAuNPs were compared to citrate-capped AuNPs after normalization. Generally, a small shift (typically less than 10 nm) of the SPR peak is the indication of successful surface modification as shown in Fig. 2a. Due to the 1 nm minimum accuracy of the UV plate reader, in some cases, the small change in SPR peak may be hard to see, but if the overall absorbance curve showed a small shift that could also be considered as a successful modification. If UV-visible spectra of PAuNPs and citrate-capped AuNPs are identical, it means that there is no interaction between polymer and AuNPs and thus no surface modification occurs (Fig. 2b). In contrast, a larger shift (>100 nm) is an indication of interparticle aggregation (Fig. 2c).<sup>87,88</sup> Thus, the observation of a small change in SPR peak with no peak in the range of 600–800 nm is deemed a successful gold surface modification with no aggregation. The wavelength of SPR peak for each of the PAuNPs is depicted in Table S1,<sup>†</sup> which gives an overview of the PAuNPs library. The heat map in Fig. 3 outlines the modification results of the PAuNPs library, showing that the successful modification rate is 57%.

According to the UV-visible results (Fig. 3), the modification of Au<sub>32</sub> with the positive polymer series, P<sub>a</sub>5k, P<sub>a</sub>10k, and P<sub>a</sub>15k, was successful for the whole range of polymer/Au mass ratios tested (from 1/9 to 9/1). However, for the modification of smaller sizes of AuNPs (Au<sub>19</sub>, Au<sub>11</sub>, and Au<sub>4</sub>), lower polymer/Au ratios (Au<sub>19</sub>, 1/9, 1/3, 1/1; Au<sub>11</sub>, 1/9, 1/3; Au<sub>4</sub>, 1/9) resulted in aggregation while higher polymer/Au ratios (Au<sub>19</sub>, 3/1, 9/1; Au<sub>11</sub>, 1/1, 3/1, 9/1; Au<sub>4</sub>, 1/3, 1/1, 3/1, 9/1) yielded satisfactory modification result. This phenomenon may be caused by the electrostatic interaction between the positive polymer and negative nanoparticles surface. With a lower P<sub>a</sub>/Au ratio, the strong affinity between opposite charges from polymer and AuNPs may lead to the interparticle aggregation. With a higher P<sub>a</sub>/Au ratio, fast combination between the thiol group of polymer and gold surface may lead to more polymer covering, which would help to avoid the interparticle aggregation because of the surface repulsion.<sup>88</sup> Au<sub>32</sub> and Au<sub>19</sub> could not be successfully modified with the negative polymer series, P<sub>b</sub>5k, P<sub>b</sub>10k, and P<sub>b</sub>15k, at any polymer/Au ratios possibly due to the electrostatic repulsion. However, successful modifications were observed for the smaller AuNPs (Au<sub>11</sub> and Au<sub>4</sub>), at higher polymer/Au ratios (1/1, 3/1, and 9/1). Likewise, the neutral polymer series, P<sub>c</sub>5k, P<sub>c</sub>10k, P<sub>c</sub>15k and P<sub>c</sub>30k, successfully modified all sizes of AuNPs in most of the polymer/Au ratios. Generally, the optimum conditions for a successful surface modification of AuNPs require medium polymer/Au ratios, which are consistent with the earlier reports.<sup>60,89,90</sup>

DLS measurements were conducted to confirm the modification results from UV-visible measurements, also using a high

Table 3 Particle sizes of citrate-capped gold nanoparticles

	$\lambda_{\text{SPR}}$ (nm)	$A_{\text{SPR}}/A_{450}$	Core diameter (nm)		
			UV	DLS	TEM
Au <sub>32</sub>	526	1.83	36	35.4 ± 2.1	31.7 ± 2.9
Au <sub>19</sub>	522	1.63	15	19.9 ± 1.3	19.0 ± 4.3
Au <sub>11</sub>	518	1.50	10	10.6 ± 2.1	10.6 ± 1.6
Au <sub>4</sub>	511	1.18	4	4.4 ± 0.9	4.4 ± 1.0

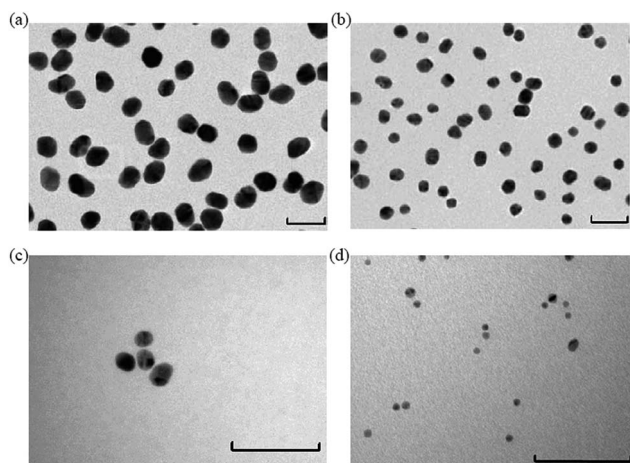


Fig. 1 TEM images of citrate-capped AuNPs: (a) Au<sub>32</sub> (b) Au<sub>19</sub> (c) Au<sub>11</sub> and (d) Au<sub>4</sub>; scale bar = 50 nm.

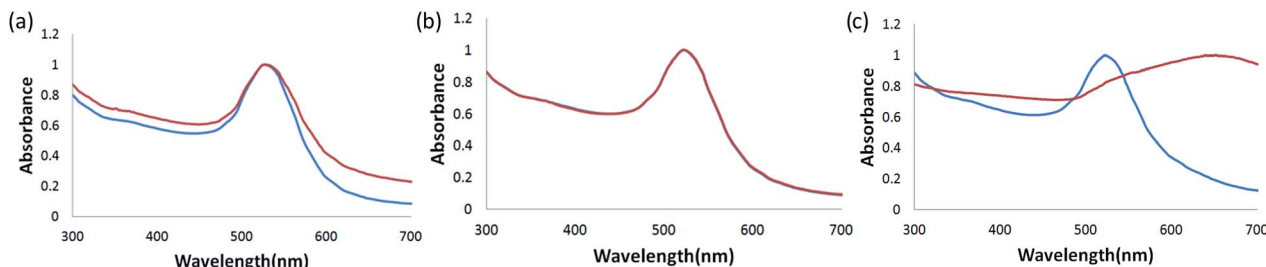


Fig. 2 Three representative UV-visible spectra of citrate-capped AuNPs (blue line) and PAuNPs (red line): (a)  $P_c5kC3-Au_{32}$ , where AuNPs surface modification was successful; (b)  $P_b5kC4-Au_{19}$ , where AuNPs surface modification failed (*i.e.* no interaction between polymer and AuNPs); (c)  $P_a10kC1-Au_{11}$ , where aggregation of AuNPs occurred; concentration of all samples is  $0.048 \text{ mg mL}^{-1}$  in deionized water.

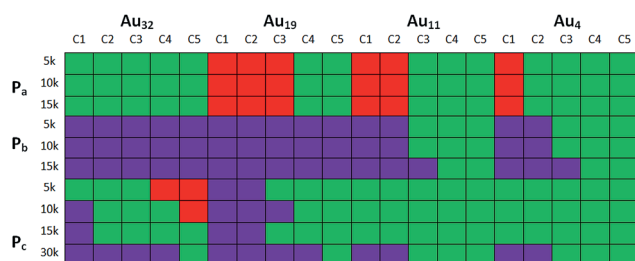


Fig. 3 Heat map showing modification results for PAuNPs library: (red) aggregation occurred; (blue) no modification occurred; (green) successful modification.

throughput Wyatt plate reader. Rather than the absolute values, variation trends of the hydrodynamic diameters were assessed in this study because a big difference was observed between the results acquired from high throughput Wyatt DLS plate reader and the normal Malvern Zetasizer DLS equipment. In general, for the samples with successful surface modification, the hydrodynamic diameters of PAuNPs slightly increase compared to original AuNPs and have low polydispersity index in particle size distribution (PD%). If the diameters increase too much compared to original citrate-capped AuNPs, it indicates that aggregation occurred, which will also be reflected by its high PD% of size distribution, sometimes having the multimodal peaks. The hydrodynamic diameters of the combinations

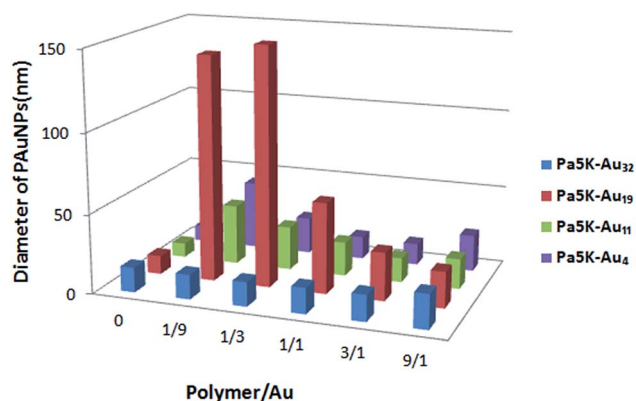


Fig. 4 Hydrodynamic diameters of  $P_a5k-AuNPs$  acquired from Wyatt plate reader: the polymer/Au ratio was 0 (C0), 1/9 (C1), 1/3 (C2), 1/1 (C3), 3/1 (C4), 9/1 (C5).

between  $P_a5k$  and 4 sizes of AuNPs using different polymer/Au ratios are depicted in Fig. 4 as an example. Among 20 samples the diameters of 6 samples ( $P_a5kC1-Au_{19}$ ,  $P_a5kC2-Au_{19}$ ,  $P_a5kC3-Au_{19}$ ,  $P_a5kC1-Au_{11}$ ,  $P_a5kC2-Au_{11}$  and  $P_a5kC1-Au_4$ ) were much larger than that of the citrate-capped AuNPs acquired by the DLS plate reader and the size distribution of those samples showed multimodal status as well, which both proved that the above PAuNPs aggregated heavily. The aggregated samples are marked with solid squares in Table S1.† These results are consistent with those obtained from UV-visible measurement. The diameters of the other samples are close to that of original AuNPs with low PD%, indicating no aggregation occurred.

The presence of the polymer layer on the nanoparticles surface can be visualized by TEM with the assistance of negative staining. Negative staining enhances the contrast between AuNPs and the polymer layer in TEM analysis and the images will show a clear white corona around the AuNPs which suggests the presence of a polymer layer.<sup>91,92</sup> Fig. 5 shows TEM image of successfully modified  $Au_{32}$  (Fig. 5b) in comparison with citrate-capped  $Au_{32}$  (Fig. 5a), where the sample  $P_c10kC3-Au_{32}$  showed a clear white corona around the gold cores.

#### Aqueous dispersion stability of PAuNPs

The biological properties of nanomaterials largely rely on their dispersion stability in aqueous media. Instability of nanoparticles aqueous dispersion leads to aggregation, which may cause toxicity to the body. Therefore, it is very important to improve aqueous dispersion stability of AuNPs and monitor their aggregation behavior prior use in biological experiments. Common methods to investigate the aggregation behavior include UV-visible, TEM, and DLS. Due to a large number of

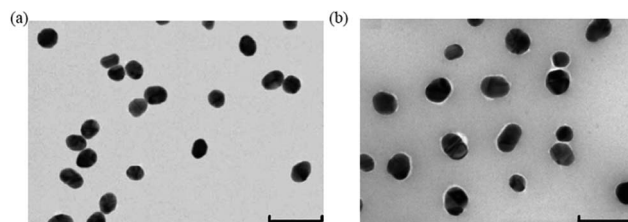


Fig. 5 TEM images with negative staining: (a) citrate-capped  $Au_{32}$ ; (b)  $P_c10kC3-Au_{32}$ ; 50 nm for all scale bars.

samples for screening in this study, the stability property of the PAuNPs library (200 formulations) has to be investigated by a high throughput technique using UV-visible spectroscopy and DLS. The limited accessibility to TEM constricts its application in this regard.

The experiments were carried out in three different media in parallel: Milli-Q water, PBS, and PBS mixed with 5 wt% BSA. The measurements were acquired at 528, 523, 519 nm for Au<sub>32</sub>, Au<sub>19</sub> and Au<sub>11</sub>, respectively. A number of PAuNPs samples were selected from the library for stability test based on the results of successful modification described above (Table 4). The selected candidates include PAuNPs synthesized using only one moderate polymer/Au ratio for each polymer, as it seemed to give the best modification outcome. Au<sub>4</sub> was not included in this experiment as its size was too small to be precipitated using centrifugation, even if a 16 000g centrifuge for 30 minutes was used. As described in experimental part, we need to use centrifugation to get concentrated PAuNPs solution, which was impossible in the case of Au<sub>4</sub>. The diluted unmodified AuNPs solution in Milli-Q water at 0 h was used as the control sample and its absorbance of SPR peak was normalized to 1. The normalized absorbance of SPR peak from selected PAuNPs solutions was compared to AuNPs control sample and the degree of nanoparticles aggregation was quantified by the absorbance ratio of PAuNPs to AuNPs (Fig. 6). In pure Milli-Q water and the mixture of PBS with 5 wt% BSA all selected PAuNPs showed negligible change in the relative absorbance of SPR peak compared to the control sample AuNPs, indicating their excellent stability in both solvents. However, the samples seemed less stable in PBS buffer as a few samples appeared to decrease in the relative absorbance of SPR peak compared to the control sample AuNPs. It was observed that the original citrate-capped AuNPs (control sample) aggregated immediately when PBS solution was added. The polymer modification, however, greatly improved the stability of modified AuNPs in PBS with an overall relative absorbance decrement in the range of 0–40% after 48 hours incubation at 37 °C. As shown in Fig. S4a–c,† positive P<sub>a</sub> modified AuNPs showed improved stability in PBS with the absorbance decrement in the range of 5–40% after 48 hours incubation at 37 °C. The negative P<sub>b</sub> modified Au<sub>11</sub> (P<sub>b</sub>5kC4-Au<sub>11</sub>, P<sub>b</sub>10kC4-Au<sub>11</sub>, and P<sub>b</sub>15kC4-Au<sub>11</sub>) exhibited excellent stability in PBS with no decrease in absorbance after

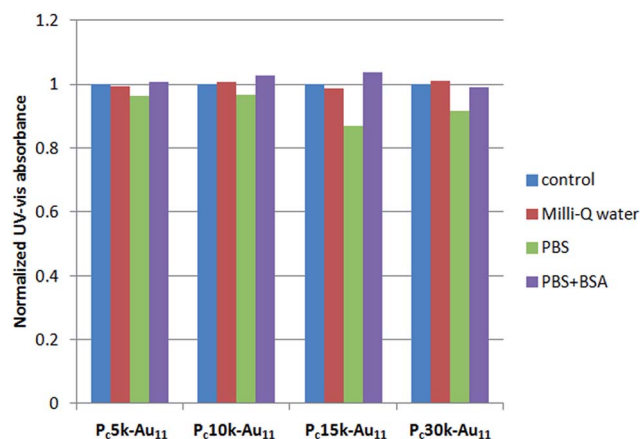


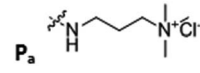
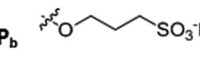
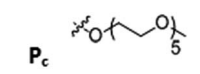
Fig. 6 Normalized UV-visible absorbance of selected PAuNPs near SPR peak after incubation for 48 hours at 37 °C in three media (the absorbance of AuNPs in Milli-Q water at  $t = 0$  was used as control); concentration of all samples is 0.12 mg mL<sup>-1</sup> in deionized water.

48 h incubation (Fig. S4d†). The P<sub>c</sub> modified AuNPs showed improved stability in PBS (Fig. 6 and Fig. S4e and f†). However, it seems that the AuNPs modified by P<sub>c</sub>10k could always produce a better result regardless of particle size, indicating that P<sub>c</sub>10k seems to be the best chain length to achieve more stable PAuNPs. In addition, it seems that the stability of smaller AuNPs (*e.g.* Au<sub>11</sub>) modified by P<sub>c</sub> was better than that of larger ones prepared under the same conditions (*e.g.* using same MW of P<sub>c</sub> and same polymer/Au ratio). As Au<sub>11</sub> modified by three different polymers showed better stability in PBS compared to Au<sub>32</sub> and Au<sub>19</sub>, and P<sub>c</sub>10k also has better performance than P<sub>c</sub>5k, P<sub>c</sub>15k, and P<sub>c</sub>30k, P<sub>a</sub>10kC4-Au<sub>11</sub>, P<sub>b</sub>10kC4-Au<sub>11</sub> and P<sub>c</sub>10kC3-Au<sub>11</sub> were selected as the best candidates for evaluation of cytotoxicity.

#### Cytotoxicity assessment of PAuNPs

Previous studies have shown that the cytotoxicity of AuNPs most likely depends on particle size, surface modification, concentration, and cell type.<sup>27</sup> Herein, the cytotoxicity of three selected candidates P<sub>a</sub>10kC4-Au<sub>11</sub>, P<sub>b</sub>10kC4-Au<sub>11</sub>, and P<sub>c</sub>10kC3-Au<sub>11</sub> against the mouse L929 cell line was evaluated *via* the MTT assays. Cell viabilities of the L929 cells after 48 hours exposure

Table 4 Selected PAuNPs for dispersion stability test

Polymer (R <sub>1</sub> )	M <sub>n</sub>	Mass ratio (polymer/Au)	Au <sub>32</sub>	Au <sub>19</sub>	Au <sub>11</sub>	
 P <sub>a</sub>	5k	3/1	P <sub>a</sub> 5kC4-Au <sub>32</sub>	P <sub>a</sub> 5kC4-Au <sub>19</sub>	P <sub>a</sub> 5kC4-Au <sub>11</sub>	
	10k		P <sub>a</sub> 10kC4-Au <sub>32</sub>	P <sub>a</sub> 10kC4-Au <sub>19</sub>	P <sub>a</sub> 10kC4-Au <sub>11</sub>	
	15k		P <sub>a</sub> 15kC4-Au <sub>32</sub>	P <sub>a</sub> 15kC4-Au <sub>19</sub>	P <sub>a</sub> 15kC4-Au <sub>11</sub>	
 P <sub>b</sub>	5k	3/1	N/A	N/A	P <sub>b</sub> 5kC4-Au <sub>11</sub>	
	10k				P <sub>b</sub> 10kC4-Au <sub>11</sub>	
	15k				P <sub>b</sub> 15kC4-Au <sub>11</sub>	
 P <sub>c</sub>	5k	1	P <sub>c</sub> 5kC4-Au <sub>32</sub>	P <sub>c</sub> 5kC3-Au <sub>19</sub>	P <sub>c</sub> 5kC3-Au <sub>11</sub>	
	10k			P <sub>c</sub> 10kC4-Au <sub>32</sub>	P <sub>c</sub> 10kC3-Au <sub>19</sub>	P <sub>c</sub> 10kC3-Au <sub>11</sub>
	15k		3/1	P <sub>c</sub> 15kC4-Au <sub>32</sub>	P <sub>c</sub> 15kC4-Au <sub>19</sub>	P <sub>c</sub> 15kC4-Au <sub>11</sub>
	30k			P <sub>c</sub> 30kC4-Au <sub>32</sub>	P <sub>c</sub> 30kC4-Au <sub>19</sub>	P <sub>c</sub> 30kC4-Au <sub>11</sub>

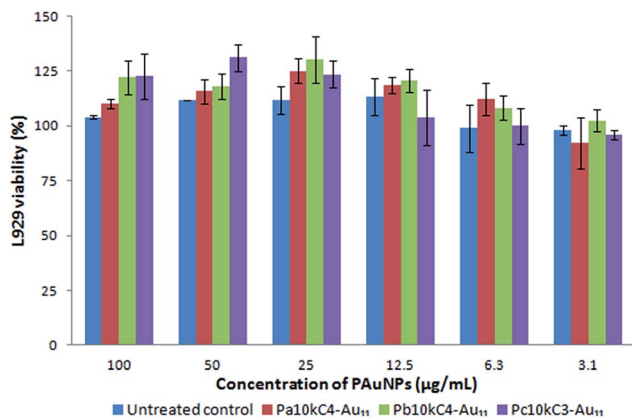


Fig. 7 Cell viability of mouse L929 cells after exposure to PAuNPs samples at different incubation concentrations for 48 hours: percentage viabilities of the treated L929 cells were expressed relative to the untreated cells (control, 100% viability), and results were all presented as mean value  $\pm$  standard deviation ( $n = 3$ ).

to the PAuNPs samples with different concentrations are summarized and shown in Fig. 7. The three synthesized PAuNPs samples induced negligible cytotoxicity after 48 hours incubation in the concentration range of 3.1–100  $\mu\text{g mL}^{-1}$ , while 10 v% DMSO treated cells showed only 2.5% viability. These results indicate a good biocompatibility of the  $\text{P}_a10\text{kC4-Au}_{11}$ ,  $\text{P}_b10\text{kC4-Au}_{11}$ , and  $\text{P}_c10\text{kC3-Au}_{11}$  samples against the L929 cell line, suggesting the potential suitability for biomedical applications.

### Evaluation of AuNPs application and development in zebrafish larvae

Having determined good biocompatibility in the cell culture system, we asked if a more complex vertebrate system would manage exposure to  $\text{P}_c10\text{kC3-Au}_{11}$  equally well. As reported by several studies, multi-sized gold nanoparticles induce non-toxicity effects in zebrafish embryos following exposure to a wide AuNPs concentration range.<sup>93–95</sup> At the meantime, some studies show that the size and surface coating affect larval development behaviour.<sup>96,97</sup> In our study, development of zebrafish larvae was analyzed after 2 days of continuous exposure to nanoparticles. Both bath application and microinjection into the cardinal vein were evaluated as application methods. The concentration range used for bath application showed no adverse developmental effects of exposure (Fig. 8A). To ensure the presence of nanoparticles in the circulatory system,  $\text{P}_c10\text{kC3-Au}_{11}$  with higher concentrations than bath application was also microinjected into the cardinal vein (Fig. 8B). A small percentage of embryos developed heart edemas and developmental defects such as tail truncation and developmental delay. The frequency of these abnormalities was found to be independent of the amount of NPs injected and therefore was likely to be caused by the microinjection procedure. Exposure to either external presence or presence of NPs in the circulatory system at the concentrations used had little effect on late development in zebrafish.

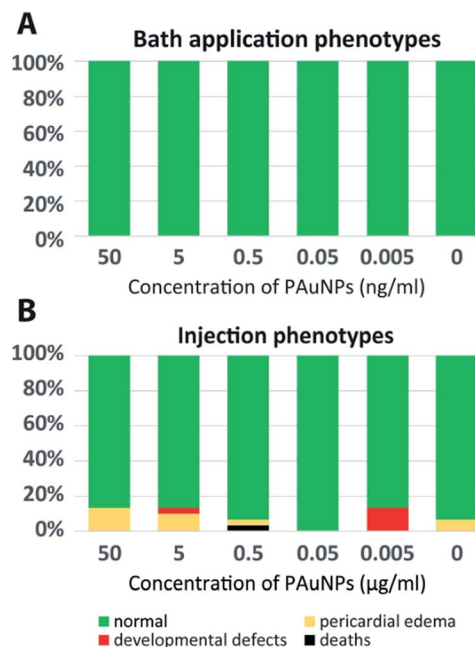


Fig. 8 Late exposure to  $\text{P}_c10\text{kC3-Au}_{11}$  had little effect on development in zebrafish larvae. (A) Phenotype distribution observed after bath application of varying concentrations of  $\text{P}_c10\text{kC3-Au}_{11}$ ,  $n = 30$ . (B) Phenotype distribution observed after intravenous injection of varying concentrations of  $\text{P}_c10\text{kC3-Au}_{11}$ ,  $n = 30$ .

The concentrations in this study were chosen with the intent to allow imaging within the dynamic range, ensuring presence of signal while avoiding saturation of signal within the region of interest. While our results confirmed earlier studies about the non-toxic qualities of gold particles in zebrafish, it is conceivable that higher concentrations of  $\text{P}_c10\text{kC3-Au}_{11}$  have effects deviating from the results shown here.<sup>90</sup> Yet, considering a pharmacological application of NPs as a drug delivery vehicle, the effective concentration would have to be determined for each particle-cargo combination which goes beyond the aim of the present work.

### Imaging of AuNPs in zebrafish larvae by synchrotron XFM beamline

Encouraged by the low developmental impact of the AuNPs presence in the vertebrate circulatory system, we set out to determine the localization of AuNPs *in vivo* by XFM using the Australian Synchrotron. This technology was particularly suited for this purpose as no modification needed to be made to the gold particles to detect them under physiological conditions. The novelty of using zebrafish at the Australian Synchrotron required us to test several methods of sample preparations and mounting (see methods). By comparing two zebrafish larva injected with PAuNPs and PBS respectively, we found that the gold signal in PAuNPs injected larvae was visualized (Fig. 9d) whilst no gold signal in PBS injected larvae was detected at all (Fig. 9c). Fig. 9a and b are the zinc elemental imaging photos showing the outlines of the larva. Those photos guide us to locate the different regions of the larva (head, trunk, etc.). Their

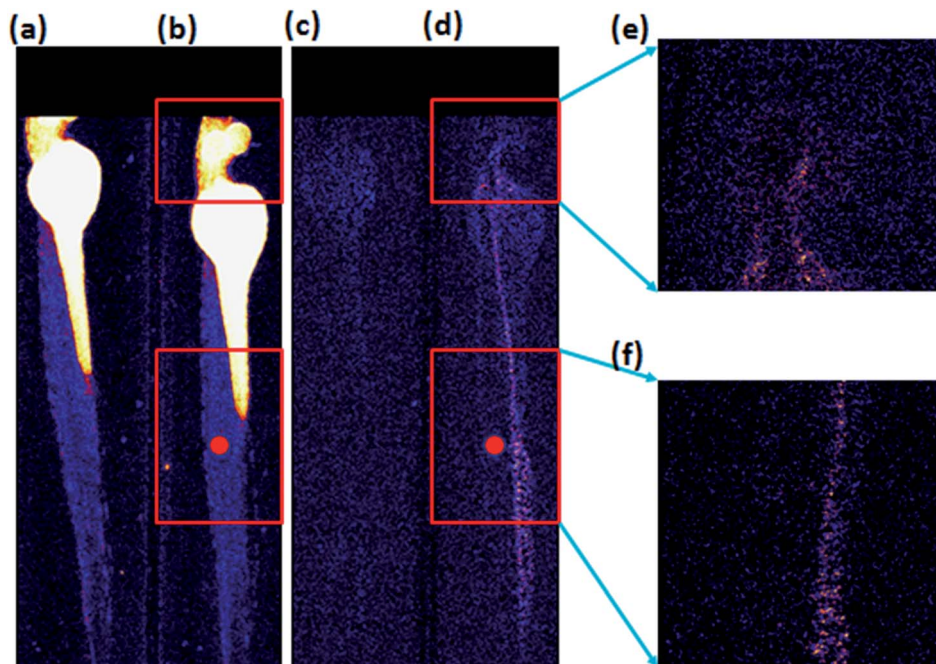


Fig. 9  $P_c10kC3-Au_{11}$  was reliably detected in the zebrafish circulatory system, red dot is the injection site. Zinc elemental imaging photos of (a) PBS injected zebrafish larvae; (b)  $P_c10kC3-Au_{11}$  injected zebrafish larvae; gold elemental imaging photos of (c) PBS injected zebrafish larvae; (d)  $P_c10kC3-Au_{11}$  injected zebrafish larvae; (e) high resolution image with PAuNPs detected in the head region; (f) high resolution image with PAuNPs detected in the lower trunk region.

corresponding gold elemental imaging photos are shown in Fig. 9c and d. Having detected the gold signal in PAuNPs injected larvae, we focused the beam on its head (Fig. 9e) and lower trunk region (Fig. 9f). By enhancing the resolution of the beam and scan time, we detected stronger gold signal intensities in both regions (Fig. 9e and f), which means a higher resolution and scan time may help to increase gold signal intensity. The gold signal appearing in the head region demonstrated that PAuNPs entered the blood system and transported into head from injection site. However, the gold signal in trunk region near the injection site (red dot in Fig. 9b) seems to be stronger than that in other regions. It is probably due to the size of fish tail which is much bigger than fish body. It is very unlikely that accumulation or aggregation of PAuNPs occurs near the injection site based on NPs dispersion stability test. In over 50% of the larvae samples, the localization of PAuNPs could be determined, limited only by the injection efficiency and the scan speed of the beamline.

As controlled samples, bath applied zebrafish larva were also imaged and gold signal could not be detected in all bath applied samples. This suggests that late oral uptake is an insufficient delivery method. This poses a problem in the context of large scale drug screening. Further modifications might be required to facilitate uptake and/or making the embryo more susceptible to uptake through changing the timing, incubation media or exposing part of the circulatory system to the environment.

This work shows that PAuNPs could be visualized in zebrafish larvae by synchrotron XFM. By utilizing synchrotron XFM, we can tell that  $P_c10kC3-Au_{11}$  particles remain in circulation

and even enter small capillaries after injection for further transportation. It is worth mentioning that the imaging signal to background is low largely due to the use of wet specimens, which results in high scatter and so background. This may be overcome by the use of dried specimens, but PAuNPs may be redistributed and therefore may not represent the real situation. Yet it remains unclear whether these particles can cross the BBB or enter cells. XFM is remarkably suited to visualize the signal of AuNPs in physiological samples without the need for extensive sample modification or preparation. Yet, to answer next series of questions, modifications to the existing XFM protocol are required, such as using it in conjunction with conventional confocal microscopy where transgenic markers and dextran coupled dyes would allow identification of blood vessels, lumen and cell bodies or an electron microscopy approach. Similarly, a recent addition to the XFM line would allow a tomography approach, increasing the resolution even further. The fact, that signal is observed in the cranial region, indicates that the particles are present in the vicinity of the developing BBB in our samples.

## Conclusions

High throughput method is an efficient way to synthesize a large amount of samples which made it possible to build up a PAuNPs library of over 200 samples in a short time.  $P_a10kC4-Au_{11}$ ,  $P_b10kC4-Au_{11}$  and  $P_c10kC3-Au_{11}$ , the three best candidates from stability screening experiments, showed no cytotoxicity based on mouse L929 cell line assay. The  $P_c10kC3-Au_{11}$  injected

zebrafish larvae were imaged using XFM beamline in Australian Synchrotron, clearly showing the gold nanoparticles visualized in the zebrafish larvae. To the best of our knowledge, this is the first report that gold elements in zebrafish larvae have been imaged using the synchrotron XFM beamline. The comparison of PAuNPs injected zebrafish larvae with control sample showed that the zebrafish larvae could be used as a potential animal model for gold imaging and might be a tractable model for investigating the ability of AuNPs to cross the BBB because of the existence of endothelial tight junction based BBB in zebrafish. These preliminary results may guide systematic research for size- and coating-dependent PAuNPs and their ability to cross the BBB. Histological study of PAuNPs injected zebrafish larvae and more analytical technologies, such as atomic absorption spectrometry (AAS) and inductively coupled plasma mass spectrometry (ICP-MS) will be used for future studies.

## Acknowledgements

We acknowledge CAS-CSIRO collaboration grant and CSC for the funding support. We also would like to thank Lynne J. Waddington (CSIRO Manufacturing) for TEM characterization and the Australian Synchrotron staff of Imaging and Medical Beamline for their help with imaging experiments. The authors also thank Drs Benjamin W. Muir, Maarten Danial, and Jie Shen (CSIRO Manufacturing) for their useful discussions.

## Notes and references

- 1 D. Strausak, J. F. Mercer, H. H. Dieter, W. Stremmel and G. Multhaup, *Brain Res. Bull.*, 2001, **55**, 175.
- 2 P. B. Verghese, J. M. Castellano and D. M. Holtzman, *Lancet Neurol.*, 2011, **10**, 241.
- 3 W. M. Pardridge, *Drug Discovery Today*, 2007, **12**, 54.
- 4 W. Kaplan, *Priority Medicines for Europe and the World: A Public Health Approach to Innovation*, World Health Organization, 2004.
- 5 B. T. Hawkins and T. P. Davis, *Pharmacol. Rev.*, 2005, **57**, 173.
- 6 N. J. Abbott, L. Rönnbäck and E. Hansson, *Nat. Rev. Neurosci.*, 2006, **7**, 41.
- 7 B. V. Zlokovic, *Neuron*, 2008, **57**, 178.
- 8 R. A. Petros and J. M. DeSimone, *Nat. Rev. Drug Discovery*, 2010, **9**, 615.
- 9 C. Sun, J. S. Lee and M. Zhang, *Adv. Drug Delivery Rev.*, 2008, **60**, 1252.
- 10 K. Riehemann, S. W. Schneider, T. A. Luger, B. Godin, M. Ferrari and H. Fuchs, *Angew. Chem., Int. Ed. Engl.*, 2009, **48**, 872.
- 11 S. M. Moghimi, A. C. Hunter and J. C. Murray, *FASEB J.*, 2005, **19**, 311.
- 12 H. S. Choi, W. Liu, P. Misra, E. Tanaka, J. P. Zimmer, B. I. Ipe, M. G. Bawendi and J. V. Frangioni, *Nat. Biotechnol.*, 2007, **25**, 1165.
- 13 J. F. Hainfeld, D. N. Slatkin and H. M. Smilowitz, *Phys. Med. Biol.*, 2004, **49**, N309.
- 14 G. F. Paciotti, L. Myer, D. Weinreich, D. Goia, N. Pavel, R. E. McLaughlin and L. Tamarkin, *Drug Delivery*, 2004, **11**, 169.
- 15 I. H. El-Sayed, X. Huang and M. A. El-Sayed, *Cancer Lett.*, 2006, **239**, 129.
- 16 G. F. Paciotti, D. G. Kingston and L. Tamarkin, *Drug Dev. Res.*, 2006, **67**, 47.
- 17 B. D. Chithrani and W. C. Chan, *Nano Lett.*, 2007, **7**, 1542.
- 18 J. D. Gibson, B. P. Khanal and E. R. Zubarev, *J. Am. Chem. Soc.*, 2007, **129**, 11653.
- 19 Y. Cheng, A. C. Samia, J. D. Meyers, I. Panagopoulos, B. Fei and C. Burda, *J. Am. Chem. Soc.*, 2008, **130**, 10643.
- 20 P. Ghosh, G. Han, M. De, C. K. Kim and V. M. Rotello, *Adv. Drug Delivery Rev.*, 2008, **60**, 1307.
- 21 E. Boisselier and D. Astruc, *Chem. Soc. Rev.*, 2009, **38**, 1759.
- 22 X. Wu, T. Ming, X. Wang, P. Wang, J. Wang and J. Chen, *ACS Nano*, 2009, **4**, 113.
- 23 B. Duncan, C. Kim and V. M. Rotello, *J. Controlled Release*, 2010, **148**, 122.
- 24 G. Sonavane, K. Tomoda and K. Makino, *Colloids Surf., B*, 2008, **66**, 274.
- 25 R. C. Van Lehn, P. U. Atukorale, R. P. Carney, Y. S. Yang, F. Stellacci, D. J. Irvine and A. Alexander-Katz, *Nano Lett.*, 2013, **13**, 4060.
- 26 S. K. Balasubramanian, J. Jittiwat, J. Manikandan, C.-N. Ong, E. Y. Liya and W.-Y. Ong, *Biomaterials*, 2010, **31**, 2034.
- 27 N. Khlebtsov and L. Dykman, *Chem. Soc. Rev.*, 2011, **40**, 1647.
- 28 A. B. Etame, C. A. Smith, W. C. Chan and J. T. Rutka, *J. Nanomed. Nanotechnol.*, 2011, **7**, 992.
- 29 D. Y. Joh, L. Sun, M. Stangl, A. Al Zaki, S. Murty, P. P. Santoemma, J. J. Davis, B. C. Baumann, M. Alonso-Basanta and D. Bhang, *PLoS One*, 2013, **8**, 62425.
- 30 D. T. Wiley, P. Webster, A. Gale and M. E. Davis, *Proc. Natl. Acad. Sci. U. S. A.*, 2013, **110**, 8662.
- 31 Y. Cheng, Q. Dai, R. A. Morshed, X. Fan, M. L. Wegscheid, D. A. Wainwright, Y. Han, L. Zhang, B. Auffinger and A. L. Tobias, *Small*, 2014, **10**, 5137.
- 32 E. Neuwelt, N. J. Abbott, L. Abrey, W. A. Banks, B. Blakley, T. Davis, B. Engelhardt, P. Grammas, M. Nedergaard and J. Nutt, *Lancet Neurol.*, 2008, **7**, 84.
- 33 R. R. Arvizo, O. R. Miranda, M. A. Thompson, C. M. Pabelick, R. Bhattacharya, J. D. Robertson, V. M. Rotello, Y. Prakash and P. Mukherjee, *Nano Lett.*, 2010, **10**, 2543.
- 34 T. S. Hauck, A. A. Ghazani and W. C. Chan, *Small*, 2008, **4**, 153.
- 35 Y.-S. Chen, Y.-C. Hung, L.-W. Lin, I. Liau, M.-Y. Hong and G. S. Huang, *Nanotechnology*, 2010, **21**, 485102.
- 36 A. K. Boal, F. Ilhan, J. E. DeRouchey, T. Thurn-Albrecht, T. P. Russell and V. M. Rotello, *Nature*, 2000, **404**, 746.
- 37 M. K. Corbierre, N. S. Cameron, M. Sutton, S. G. J. Mochrie, L. B. Lurio, A. Ruehm and R. B. Lennox, *J. Am. Chem. Soc.*, 2001, **123**, 10411.
- 38 N. Nath and A. Chilkoti, *Adv. Mater.*, 2002, **14**, 1243.
- 39 Y. C. Cao, R. Jin and C. A. Mirkin, *Science*, 2002, **297**, 1536.
- 40 J. Raula, J. Shan, M. Nuopponen, A. Niskanen, H. Jiang, E. I. Kauppinen and H. Tenhu, *Langmuir*, 2003, **19**, 3499.

- 41 J. Ouyang, C.-W. Chu, C. R. Szmanda, L. Ma and Y. Yang, *Nat. Mater.*, 2004, **3**, 918.
- 42 M.-Q. Zhu, L.-Q. Wang, G. J. Exarhos and A. D. Q. Li, *J. Am. Chem. Soc.*, 2004, **126**, 2656.
- 43 J. Du, Y. Tang, A. L. Lewis and S. P. Armes, *J. Am. Chem. Soc.*, 2005, **127**, 17982.
- 44 Y. Kang and T. A. Taton, *Angew. Chem., Int. Ed.*, 2005, **44**, 409.
- 45 H. Dong, M. Zhu, J. A. Yoon, H. Gao, R. Jin and K. Matyjaszewski, *J. Am. Chem. Soc.*, 2008, **130**, 12852.
- 46 J. Du, Y. Sun, L. Jiang, X. Cao, D. Qi, S. Yin and X. Chen, *Small*, 2011, **7**, 1407.
- 47 Y. Zhao, Z. Wang, W. Zhang and X. Jiang, *Nanoscale*, 2010, **2**, 2114.
- 48 N. Nath and A. Chilkoti, *J. Am. Chem. Soc.*, 2001, **123**, 8197.
- 49 M.-Q. Zhu, L.-Q. Wang, G. J. Exarhos and A. D. Li, *J. Am. Chem. Soc.*, 2004, **126**, 2656.
- 50 M. K. Corbierre, N. S. Cameron and R. B. Lennox, *Langmuir*, 2004, **20**, 2867.
- 51 Y. Kang and T. A. Taton, *Macromolecules*, 2005, **38**, 6115.
- 52 R. Jin, *Nanoscale*, 2010, **2**, 343.
- 53 D. Li, Q. He, Y. Cui and J. Li, *Chem. Mater.*, 2007, **19**, 412.
- 54 H. Duan, M. Kuang, D. Wang, D. G. Kurth and H. Möhwald, *Angew. Chem., Int. Ed. Engl.*, 2005, **44**, 1717.
- 55 H. Skaff and T. Emrick, *Chem. Commun.*, 2003, 52.
- 56 D. Kim, S. Park, J. H. Lee, Y. Y. Jeong and S. Jon, *J. Am. Chem. Soc.*, 2007, **129**, 7661.
- 57 C. L. McCormick and A. B. Lowe, *Acc. Chem. Res.*, 2004, **37**, 312.
- 58 C. Boyer, V. Bulmus, T. P. Davis, V. Ladmiral, J. Liu and S. Perrier, *Chem. Rev.*, 2009, **109**, 5402.
- 59 C. T. Nguyen, T. H. Tran, X. Lu and R. M. Kasi, *Polym. Chem.*, 2014, **5**, 2774.
- 60 F. Qie, A. Astolfo, M. Wickramaratna, M. Behe, M. D. Evans, T. C. Hughes, X. Hao and T. Tan, *Nanoscale*, 2015, **7**, 2480.
- 61 G. J. Lieschke and P. D. Currie, *Nat. Rev. Genet.*, 2007, **8**, 353.
- 62 G. Kari, U. Rodeck and A. P. Dicker, *Clin. Pharmacol. Ther.*, 2007, **82**, 70.
- 63 J. F. Amatruda, J. L. Shepard, H. M. Stern and L. I. Zon, *Cancer Cell*, 2002, **1**, 229.
- 64 K. Dooley and L. I. Zon, *Curr. Opin. Genet. Dev.*, 2000, **10**, 252.
- 65 D. J. Grunwald and J. S. Eisen, *Nat. Rev. Genet.*, 2002, **3**, 717.
- 66 J.-Y. Jeong, H.-B. Kwon, J.-C. Ahn, D. Kang, S.-H. Kwon, J. A. Park and K.-W. Kim, *Brain Res. Bull.*, 2008, **75**, 619.
- 67 G. Frens, *Nature*, 1973, **241**, 20.
- 68 X. Mulet, D. F. Kennedy, C. E. Conn, A. Hawley and C. J. Drummond, *Int. J. Pharm.*, 2010, **395**, 290.
- 69 J. Liu, C. Detrembleur, M. Hurtgen, A. Debuigne, M. C. De Pauw-Gillet, S. Mornet and C. Jérôme, *Polym. Chem.*, 2014, **5**, 5289.
- 70 J. Liu, C. Detrembleur, M. C. De Pauw-Gillet, S. Mornet, E. Dugué and C. Jérôme, *Polym. Chem.*, 2014, **5**, 799.
- 71 M. Westerfield, *The zebrafish book. A guide for the laboratory use of zebrafish (Danio rerio)*, Univ. of Oregon Press, Eugene, 4th edn, 2000.
- 72 C. Cianciolo Cosentino, B. L. Roman, I. A. Drummond and N. A. Hukriede, *J. Visualized Exp.*, 2010, **42**, 2079.
- 73 D. Paterson, M. D. De Jonge, D. L. Howard, W. Lewis, J. McKinlay, A. Starritt, M. Kusel, C. G. Ryan, R. Kirkham, G. Moorhead and D. P. Siddons, *AIP Conf. Proc.*, 2011, **1365**, 219.
- 74 M. J. Pushie, I. J. Pickering, M. Korbas, M. J. Hackett and G. N. George, *Chem. Rev.*, 2014, **114**, 8499.
- 75 M. Korbas, S. R. Blechinger, P. H. Krone, I. J. Pickering and G. N. George, *Proc. Natl. Acad. Sci. U. S. A.*, 2008, **105**, 12108.
- 76 M. Korbas, T. C. MacDonald, I. J. Pickering, G. N. George and P. H. Krone, *ACS Chem. Biol.*, 2011, **7**, 411.
- 77 B. F. G. Popescu, M. J. George, U. Bergmann, A. V. Garachtchenko, M. E. Kelly, R. P. E. McCrea, K. Luning, R. M. Devon, G. N. George, A. D. Hanson, S. M. Harder, L. D. Chapman, I. J. Pickering and H. Nichol, *Phys. Med. Biol.*, 2009, **54**, 651.
- 78 S. A. James, D. E. Myers, M. D. de Jonge, S. Vogt, C. G. Ryan, B. A. Sexton, P. Hoobin, D. Paterson, D. L. Howard, S. C. Mayo, M. Altissimo, G. F. Moorhead and S. W. Wilkins, *Anal. Bioanal. Chem.*, 2011, **401**, 853.
- 79 A. Grubman, S. A. James, J. James, C. Duncan, I. Volitakis, J. L. Hickey, P. J. Crouch, P. S. Donnelly, K. M. Kanninen, J. R. Liddell, S. L. Cotman, M. D. de Jonge and A. R. White, *Chem. Sci.*, 2014, **5**, 2503.
- 80 C. G. Ryan, D. P. Siddons, R. Kirkham, P. A. Dunn, A. Kuczewski, G. Moorhead, G. De Geronimo, D. J. Paterson, M. D. de Jonge, R. M. Hough, M. J. Lintern, D. L. Howard, P. Kappen and J. S. Cleverley, *AIP Conf. Proc.*, 2010, **1234**, 9.
- 81 R. Kirkham, P. A. Dunn, A. Kuczewski, D. P. Siddons, R. Dodanwela, G. Moorhead, C. G. Ryan, G. De Geronimo, R. Beuttenmuller, D. Pinelli, M. Pfeffer, P. Davey, M. Jensen, D. J. Paterson, M. D. de Jonge, M. Kusel and J. McKinlay, *AIP Conf. Proc.*, 2010, **1234**, 240.
- 82 G. Moad, E. Rizzardo and S. H. Thang, *Aust. J. Chem.*, 2005, **58**, 379.
- 83 G. Moad, E. Rizzardo and S. H. Thang, *Polymer*, 2008, **49**, 1079.
- 84 W. Haiss, N. T. Thanh, J. Aveyard and D. G. Fernig, *Anal. Chem.*, 2007, **79**, 4215.
- 85 J. Lipka, M. Semmler-Behnke, R. A. Sperling, A. Wenk, S. Takenaka, C. Schleh, T. Kissel, W. J. Parak and W. G. Kreyling, *Biomaterials*, 2010, **31**, 6574.
- 86 B. N. Khlebtsov and N. G. Khlebtsov, *Colloid J.*, 2011, **73**, 118.
- 87 S. K. Ghosh and T. Pal, *Chem. Rev.*, 2007, **107**, 4797.
- 88 M. I. Gibson, M. Danial and H.-A. Klok, *ACS Comb. Sci.*, 2011, **13**, 286.
- 89 W. Zhao, M. A. Brook and Y. Li, *ChemBioChem*, 2008, **9**, 2363.
- 90 J. Manson, D. Kumar, B. J. Meenan and D. Dixon, *Gold Bull.*, 2011, **44**, 99.
- 91 C. E. Hall, *J. Biophys. Biochem. Cytol.*, 1955, **1**, 1.
- 92 Y. Liu, X. Hao, L. J. Waddington, J. Qiu and T. C. Hughes, *Aust. J. Chem.*, 2014, **67**, 151.
- 93 B. Ofek, R. M. Albrecht, V. E. Fako and D. Y. Furgeson, *Small*, 2009, **5**, 1897.
- 94 L. M. Browning, K. J. Lee, T. Huang, P. D. Nallathamby, J. E. Lowman and X. N. Xu, *Nanoscale*, 2009, **1**, 138.
- 95 P. V. Asharani, Y. Lianwu, Z. Gong and S. Valiyaveetil, *Nanotoxicology*, 2011, **5**, 43.

- 96 L. Truong, K. S. Sali, J. M. Miller, J. E. Hutchison and R. L. Tanguay, *Comp. Biochem. Physiol., Part C: Toxicol. Pharmacol.*, 2012, **155**, 269.
- 97 L. Truong, S. C. Tilton, T. Zaikova, E. Richman, K. M. Waters, J. E. Hutchison and R. L. Tanguay, *Nanotoxicology*, 2013, **7**, 192.